Altered pseudostratified epithelial development of the lateral ventricle choroid plexus in *Mllt11* mutants

Samantha A. Moore[1], Danielle Stanton-Turcotte[1], and Angelo Iulianella[1]*

[1] Department of Medical Neuroscience, Faculty of Medicine, Dalhousie University, and Brain Repair Centre, Life Science Research Institute
1348 Summer Street, Halifax, Nova Scotia, B3H-4R2, Canada

*Correspondence: angelo.iulianella@dal.ca

Funding: The AI lab is supported by grants from NSERC (RGPIN-2020-03925) and CIHR (PJT-388914). SAM was supported by a CIHR MSc scholarship award.

Author contributions: SM and DST conducted experiments, SM and AI co-wrote the manuscript, DST and AI edited figures, AI secured funding and supervised project.

Abbreviations: Cortical Hem (CH), Choroid Plexus (ChP), Subventricular Zone (SVZ), Neuroepithelial Progenitors (NEPs).

Key words: Choroid plexus, cuboidal epithelia, Cortical Hem, Otx1/2, Cux2, Mllt11, migration.

ABSTRACT

The choroid plexuses (ChPs) are modified epithelial structures that penetrate all four cerebral ventricles and secrete cerebrospinal fluid. They consist of a central stroma that is vascularized with fenestrated blood vessels and connective tissue. The ChPs are of dual embryonic origin, with forebrain neuroepithelial cells contributing to the epithelial component and mesenchymal cells contributing to the stromal cells. The growth of the ChPs into the ventricular spaces is fueled by the migration and proliferation of neuroepithelial progenitor cells originating from the cortical hem. However, the genetic regulation of NEP migration during ChP development is not well understood. Here we report the role of Mllt11 (Af1q/Tcf7c) in regulating the formation of the ChP principally by regulating the migration of Otx1/2^{+} NEPs into the base of the fetal ChP, fueling its growth into the lateral ventricle. We also describe that *Mllt11* mutants displayed a loss of the cuboid epithelial architecture of the ChP, altering the pseudostratified epithelial organization of the outer layers of the ChP.

INTRODUCTION

The Choroid Plexus (ChP) of the lateral ventricle is one of the main sources of cerebrospinal fluid but its development remains a relatively understudied process. Recent work has shown that ChP formation is underlain by complex morphogenetic processes dependent on the patterning of telencephalic midline structures (Ghersi-Egea et al., 2018; Liddelow, 2015; Moore and Iulianella, 2021). The ChPs are modified epithelial structures that protrude into all four cerebral ventricles. They consist of a central stroma that is highly vascularized interdigitated with fenestrated leaky blood vessels and connective tissue (Johansson, 2014). The initial development of the ChPs begins around embryonic day (E)11 and is largely complete by E14 in the mouse, with the fourth hindbrain ventricular region ChP being the first to differentiate, followed by the lateral ventricular ChPs, and that of the remaining ventricles (Dziegielewska et al., 2001). The ChPs are of dual embryonic origin, as neuroepithelial progenitor cells (NEPs) from the cortical hem (CH) region give rise to the epithelial component and cephalic mesenchymal cells establish the stromal component (Johansson, 2014; Lun et al., 2015; Moore and Iulianella, 2021).

The differentiation of the ChP from NEPs follows a series of morphogenetic events characteristic of pseudostratified epithelial tissues (Moore and Iulianella, 2021). Epithelial cells change to columnar epithelium with apically located nuclei and an emerging basal connective tissue with sparse villi-like extensions. This is followed by a flattening of the outer ChP epithelial cells to become more cuboidal in shape, with centrally or apically located nuclei and more complex villi (Ek et al., 2003). Epithelial cells are sequentially added from a proliferative ventricular zone (VZ) located at the 'root' of each plexus as they transition through the stages outlined above (Liddelow et al., 2010). NEPs originating from the VZ are "pushed" out from the root of the ChP in the upper (dorsal) arm by newly divided cells and migrate towards the tip of the stalk. Thus, the ChP is an excellent model for epithelial differentiation during development and plays a crucial role in regulating brain function and neural stem cell maintenance (Moore and Iulianella, 2021). Yet our understanding of the genetic processes that regulate the migration of NEPs during ChP formation remains rudimentary.

Here we report a role for Mllt11/Af1q/Tcf7c (Myeloid/lymphoid or mixed-lineage leukemia; translocated to chromosome 11; also known as All1 Fused Gene from Chromosome 1q or Tcf7 co-factor) in regulating ChP formation. Work from our laboratory has identified

Mllt11 as a regulator of migration of neurons in the developing cortical superficial layer, cerebellar granule cells, and retinal neuroblasts (Blommers et al., 2023; Blommers et al., 2024; Stanton-Turcotte et al., 2022; Yamada et al., 2014). During these investigations, we observed abnormal ChP morphology in the developing lateral ventricle of *Mllt11* conditional knockout (cKO) neonatal mice. Given its role in neuronal migration we hypothesized that *Mllt11* may also control NEP migration contributing to ChP growth into the lateral ventral. We used the *Cux2*$^{iresCre/+}$ driver line to inactivate *Mllt11* in the developing mouse embryonic CH, which gives rise to the lateral ventricle ChP (Fregoso et al., 2019; Moore and Iulianella, 2021; Yamada et al., 2015), using an *Mllt11*$^{flox/flox}$ mouse line we previously described (Stanton-Turcotte et al., 2022). EdU birth dating and tdTomato^{+} fate mapping analysis suggests the truncated lateral ventricle ChP in the *Mllt11* null mutants was largely due to a migratory defect of Otx1/2^{+} ChP progenitors in the CH neuroepithelium. This was associated with a change in the typical stratified epithelial organization of the ChP, with cells abnormally pushed inwards towards the ChP core instead of aligning into straight pseudostratified columns along its ventricular surface. Altogether, these findings suggest a role for Mllt11 in the migration of ChP NEPs and cytoarchitectural organization of the epithelium lining the ChP.

MATERIALS AND METHODS

Animals.

Mice used in this study were handled in accordance with the regulations of the Dalhousie animal ethics committee and the guidelines of the Canadian Council on Animal Care. The generation of *Cux2*$^{iresCre/+}$*; Mllt11*$^{Flox/Flox}$: Ai9 tdTomato reporter (B6.Cg-*Gt(ROSA)26Sor*$^{tm9(CAG-tdTomato)Hze}$/J, 007909, The Jackson Laboratory) conditional mouse mutants was described previously (Stanton-Turcotte et al., 2022). In the forebrain, the *Cux2* locus-driven Cre expression results in the inactivation of *Mllt11* and expression of *tdTomato* in neurogenic progenitors, superficial cortical neurons, and CH and its derivatives, including the ChP (Fregoso et al., 2019; Stanton-Turcotte et al., 2022; Yamada et al., 2015). All experiments were performed with *Cux2*$^{iresCre/+}$*; Ai9; Mllt11*$^{+/+}$ as the wild-type (WT) control, and *Cux2*$^{iresCre/+}$*; Ai9; Mllt11*$^{flox/flox}$ as the conditional knockout (cKO), harvested at E14.5 and E18.5.

Histology and immunohistochemistry.

Brains were dissected out and fixed in 4% paraformaldehyde (PFA), equilibrated in sucrose, and embedded in Optimum Cutting Temperature compound (Tissue-Tek, Torrance, CA). A total of 40 coronal sections per embryo at 12µm per section. Immunohistochemistry was conducted on fetal brains as previously described (Iulianella et al., 2008; Stanton-Turcotte et al., 2022). Primary antibodies used were rabbit anti-Otx1/2 (1:500, Abcam ab21990), rabbit anti-Lhx2 (1:500; Abcam ab184337), rabbit anti-Pals1 (1:300, Proteintech 1771-1-AP), mouse anti-ZO1 (1:100, Invitrogen 339100). Donkey anti-mouse and anti-rabbit highly cross absorbed AlexaFluor 488 or 647 secondary antibodies (1:1500, Invitrogen) were used to detect primary antibodies. Images were captured using a Zeiss AxioObserver inverted fluorescent microscope with x20 and x40 oil objectives and Apotome 2 Structural Illumination. Montages were assembled using Photoshop (Adobe, San Jose, CA).

EdU (5-ethynyl-2´-deoxyuridine) labeling.

10 mM EdU solution was prepared in DMSO and administered via intraperitoneal injection into dams. EdU was dosed at 30 mg/kg body in a solution of 10 mg/ml PBS. Mice were dosed at E14.5 and harvested at E18.5 and EdU staining was conducted using Click-iT EdU imaging kit (Invitrogen). The immunohistochemistry protocol was adapted such that EdU staining was performed before the addition of anti-Otx1/2 primary antibodies, as described previously (Blommers et al., 2023).

Sampling methodology and statistics.

Analysis of the CH region including the dentate neuroepitheliul (DNE) and ChP stalk at E14.5 was restricted to 50 µm x 50 µm counting frames. For the ChP, the 50 μm^2 frames were placed at the base of the ChP stalk and along the length of the stalk. Analysis of cell polarity was performed in 100µm x 50µm bins placed randomly along distal and proximal regions of the ChP. Cells positively labeled with each IHC marker were counted within counting frames or analyzed for fluorescence density within bins using ImageJ (FIJI) (Schindelin et al., 2012), and statistical analyses were performed using PRISM (GraphPad). Statistical significance was obtained by performing unpaired Student's t-tests (two-tailed) to compare the means and standard error of the mean (SEM) between the WT and cKO data sets, with significance level set at $P \leq 0.05$ (*$P \leq 0.05$, **$P \leq 0.01$, ***$P \leq 0.001$, ****$P \leq 0.0001$). For all experiments, n of 3-6 WT and cKO

individuals were analyzed and cell counts were reported as mean ± SEM. Cell counts were performed blinded to genotype and data was presented as scatter boxplots or bar graphs with each point representing individual embryos.

RESULTS AND DISCUSSION

The CH region forms a specialized nexus at the tip of the pallial cortex that is enriched in signaling proteins and transcription factors that act to pattern telencephalon along into medial-lateral, and ventral–dorsal axes (Moore and Iulianella, 2021). Lhx2 acts as a selector gene for cerebral cortical fate and plays a critical role in patterning the forebrain midline and CH (Bulchand et al., 2001; Monuki et al., 2001; Roy et al., 2014). We therefore used Lhx2 to assess issues with the developing dorsal telencephalic midline neuroepithelium (DNE, Fig. 1A-B). We noted an elevated number of Lhx2$^+$ cells at E14.5 within the SVZ in the *Mllt11* conditional knockout (cKO) relative to the wild type (WT) controls (p=0.0004; n=6; Fig. 1C). Since Lhx2 is critical in establishing accurate boundary region between the dorsal telencephalon and CH, we examined whether there were any notable changes CH region by staining for the homeodomain transcription factor Otx2, which regulates the formation the anterior-most forebrain regions, including the CH (Johansson et al., 2013). We used an antibody that detects both Otx1 and Otx2 (Otx1/2) to demarcate NEPs in the CH and ChP. We noted that the CH area, outlined by the hatched yellow line, was significantly smaller in the *Mllt11* cKOs relative to control fetal brains (p=0.003; n=6) (Figure 1D-F). This suggested that *Mllt11* loss led to a slightly reduced CH region, which may have affected the numbers of NEPs that migrate during ChP growth. The conditional strategy removed *Mllt11* and activated *tdTomato* expression from the Ai9 reporter mouse allele (Stanton-Turcotte et al., 2022), allowing for the fate-mapping of Cux2$^+$ cells in the CH and its derivatives, including the entire ChP stalk (Fig.1G, H) (Fregoso et al., 2019; Stanton-Turcotte et al., 2022; Yamada et al., 2015). We observed decreased tdTomato$^+$ cell staining entering the base of the developing ChP stalk in *Mllt11* cKO mutants relative to WTs (white arrowheads, Fig. 1G, H), suggesting a migration defect.

Mllt11 Loss Decreased ChP Stalk Length

To evaluate the effect of *Mllt11* loss on ChP development, we focused our analysis at E14.5 when ChP formation in the lateral ventricle peaks and used Otx1/2 immunostaining to

outline the CH and ChP in our morphometric analyses (Johansson et al., 2013). The ChP stalk length was significantly shorter in the *Mllt11* cKOs (407.1 ± 22.95μm; n=8) relative to WTs (540.1 ± 27.04; p<0.0001; Figure 2A-C). *Mllt11* cKO mutants displayed thicker ChP stalks in fate-mapping and immunostaining experiments (Figs. 1H, 2B), and we noted an average increase of ChP stalk thickness of approximately 3μm, which did not reach statistically significant difference between cKOs (29.33 ± 1.57μm; n=8) and WT controls (26.17 ± 0.93μm; n=8; p=0.10; Fig. 2A, B, D). This suggested that *Mllt11* loss from CH NEPs led to altered ChP neuroepithelial cytoarchitecture, but the cellular mechanisms for this phenotype was unclear. We observed an abnormal clustering of Otx1/2$^+$ cells at the base of ChP along the ventricular surface relative to the distal tip 350 μm away (Fig. 2E), likely reflecting aberrant migration of *Mllt11* mutant NEPs (Fig. 2E).

Mllt11 loss affected the organization of the ChP basement membrane

The aberrant cellular morphology of the ChP stalk in *Mllt11* cKOs fetal brains, led us to examine the pseudostratified architecture of the epithelial component of the stalk using the basement membrane marker *Zona Occludens*-1 (ZO-1) antibodies. ZO-1 is normally expressed in epithelial and endothelial cells and acts as a scaffold protein cross-linking and anchoring tight junctions (McNeil et al., 2006). Importantly, we noted a marked change in the typical cuboidal epithelial organization of the maturing ChP stalk in the E18.5 *Mllt11* cKOs, with mutant cells clustering aberrantly along the width of the ChP (Fig. 3C; arrowheads in Fig. 3D), instead of being arrayed in single file along the ChP stalk length as in WT controls (Fig. 3A, B). The *Mllt11* mutant ChP displayed more bridging between displaced individual cells, outlined by the ectopic ZO-1 boundary staining along the width of the ChP (arrowheads, Fig. 3D). This suggested that *Mllt11* loss affected the formation of epithelial cell boundaries of the ChP stalk.

Aberrant migration of ChP NEPs in _Mllt11_ cKO mutants

To directly assess whether the truncated ChP in the *Mllt11* mutants reflected reduced migration of Otx1/2 NEPs from the CH ventricular region, we pulsed dams with the DNA analog EdU at E14.5 to label newly divided NEPs contributing the ChP formation, assessed at E18.5. We observed a significant decrease in the overall numbers of Otx1/2$^+$/EdU$^+$ cells in the cKO ChP at E18.5 (p=0.015, n=3; Fig. 3E-J). Moreover, cKOs displayed decreased EdU$^+$ NEPs populating

the distal tip of the ChP stalk (green open arrow, Fig. 3H). The ChP is composed of two neuroepithelial arms: the dorsal and ventral. NEPs migrate from the CH ventricular region and first enter the dorsal arm of the ChP (solid green arrowheads, Fig. 3H), to eventually loop around and invade the ventral arm (open green arrowheads, Fig. 3H). If *Mllt11* loss affects NEP migration, then we expect to find reduced numbers of EdU^+ entering the ventral arm of the ChP at fetal stages. We quantified the numbers of $Otx1/2^+/EdU^+$ in the dorsal and ventral arms and found greater numbers of double-labeled cells in the dorsal arm of the *Mllt11* cKO ChP, along with a corresponding decrease in the ventral arm (Fig. 3F).

Mllt11 cKO mutants did not exhibit altered epithelial polarity within the lateral ventral choroid plexus

Mllt11 loss led to a migration defect in ChP NEPs contributing to a shortening of the ChP stalk length. In addition, the mutants displayed disorganized epithelial organization in the ChP stalk, with a loss of cuboidal architecture, possibly reflecting a cell migration defect or alternatively due to a cell polarity organization defect. To explore this possibility we stained for Pals1 (Protein associated with Lin Seven 1), a protein that is asymmetrically expressed in epithelial cells, including the choroid plexus (Christensen et al., 2018; Ozcelik et al., 2010). We that the overall organization of Pals1 staining in the ChP epithelium was similar in both control and *Mllt11* cKO lateral ventricle, with staining restricted to the outer edge of the choroid stalk (Fig. 4A). However, *Mllt11* cKOs displayed a thickened outer choroid epithelium, reflecting the loss of cuboid cytoarchitecture observed in control fetal brains (insets, Fig. 4A). There was a trend towards reduced proximal ChP area staining for Pals1 in the cKOs, although the differences were not statistically significant (Fig. 4B, C). Our morphometric analyses confirmed significantly increased thickness in the proximal ChP stalk of *Mllt11* cKO mutants (24.99µm ± 1.37; n=4, vs. controls: 15.08µm ± 0.81; n=4; p= 0.002; Fig. 4F), but not distal stalk (Fig. 4G). This difference in thickness along the proximo-distal axis of the stalk is consistent with an CH NEP migration defect and explained why the average ChP thickness did not reach statistical significance (Fig. 2D). The aberrant accumulation of cells in the proximal stalk was supported by $tdTomato^+$ fate labeling (Fig. 1G, H) and EdU^+ birth dating studies (Fig. 3E-J), indicating that *Mllt11* loss primarily impacted the migration NEPs fueling the growth of the ChP stalk, resulting in truncated ChP stalks with thickened and disorganized epithelia.

Conclusions

The ChP epithelium develops from CH region generating a highly organized tissue that acts as an interface between the peripheral circulation and the CNS (Ek et al., 2003; Grove et al., 1998; Liddelow et al., 2010). We now report that *Mllt11* loss from the CH neural progenitor region resulted in a significantly truncated ChP with notable defects in its epithelial morphology. In mouse fetuses the ChP epithelium consists of a pseudostratified structure that varies from simple columnar to cuboidal organization (Huang et al., 2009; Liddelow et al., 2010). The ChP undergoes an intriguing distal-proximal maturation process whereby proliferative cells are added to the root of the plexus, forming in a "conveyor belt" like manner (Liddelow et al., 2010). A small population of proliferative cells within the root continue to divide and contribute to the epithelial component of the ChP along the length of the stalk (Huang et al., 2009; Liddelow et al., 2010). As the epithelium progresses from the proliferative pseudostratified progenitor population along the ventricular surface of the CH region, it transitions from a columnar epithelium into a highly polarized cuboidal epithelium necessary for important barrier functions (Ek et al., 2003; Liddelow et al., 2010). However, *Mllt11* cKOs displayed a loss of the cuboidal organization of epithelial cells along the length of the ChP stalk, with epithelial cells losing their polarized stratified organization. *Mllt11* mutant cells were abnormally juxtaposed with one another along the short axis of the ChP, creating ectopic cell boundaries in the epithelial layer, which were outlined by the basement membrane marker ZO-1 and the asymmetric determinant Pals1. The abnormal distribution of ZO-1^{+} and Pals1^{+} epithelial cell boundaries in the *Mllt11* mutant ChP stalk is consistent with our previous findings that Mllt11 is a novel cytoskeletal-associated protein required for neuronal migration in the cortex (Stanton-Turcotte et al., 2022), retina (Blommers et al., 2023), and cerebellum (Blommers et al., 2024).

Additionally, EdU birth dating experiments revealed reduced numbers of cells reaching the ventral arm of the ChP stalk in the cKOs, suggesting a defect in the migration of newly born Otx1/2^{+} NEPs, which ultimately translated into reduced stalk length. The reduced ChP length in *Mllt11* mutant brains could also be due to the slightly reduced CH progenitor region, which would lead to fewer NEPs invading the growing ChP, as suggested by the *Cux2*$^{ireCre/+}$*; Ai9* tdTomato^{+}-fate mapping data. Another factor contributing to shorted ChPs may be the altered epithelial cytoarchitecture of cKO stalks, with epithelial cells aberrantly juxtaposed towards the

core of the ChP stalk, instead of stacking on top of each other to form a single layer of pseudostratified epithelium.

ACKNOWLEDGMENTS

We acknowledge funding from the National Research and Engineering Council of Canada (NSERC RGPIN-2020-03925) and Canadian Institutes of Health Research (PJT-388914). SAM was supported by a CIHR MSc award.

REFERENCES

Blommers, M., Stanton-Turcotte, D. and Iulianella, A. (2023). Retinal neuroblast migration and ganglion cell layer organization require the cytoskeletal-interacting protein Mllt11. *Dev Dyn* **252**, 305-319.

Blommers, M., Stanton-Turcotte, D., Witt, E. A., Heidari, M. and Iulianella, A. (2024). Cerebellar granule cell migration and folia development require Mllt11/Af1q/Tcf7c. *Dev Neurobiol* **84**, 74-92.

Bulchand, S., Grove, E. A., Porter, F. D. and Tole, S. (2001). LIM-homeodomain gene Lhx2 regulates the formation of the cortical hem. *Mech Dev* **100**, 165-75.

Christensen, I. B., Mogensen, E. N., Damkier, H. H. and Praetorius, J. (2018). Choroid plexus epithelial cells express the adhesion protein P-cadherin at cell-cell contacts and syntaxin-4 in the luminal membrane domain. *Am J Physiol Cell Physiol* **314**, C519-C533.

Dziegielewska, K. M., Ek, J., Habgood, M. D. and Saunders, N. R. (2001). Development of the choroid plexus. *Microsc Res Tech* **52**, 5-20.

Ek, C. J., Habgood, M. D., Dziegielewska, K. M. and Saunders, N. R. (2003). Structural characteristics and barrier properties of the choroid plexuses in developing brain of the opossum (Monodelphis Domestica). *J Comp Neurol* **460**, 451-64.

Fregoso, S. P., Dwyer, B. E. and Franco, S. J. (2019). Lmx1a drives Cux2 expression in the cortical hem through activation of a conserved intronic enhancer. *Development* **146**, dev170068.

Ghersi-Egea, J. F., Strazielle, N., Catala, M., Silva-Vargas, V., Doetsch, F. and Engelhardt, B. (2018). Molecular anatomy and functions of the choroidal blood-cerebrospinal fluid barrier in health and disease. *Acta Neuropathol* **135**, 337-361.

Grove, E. A., Tole, S., Limon, J., Yip, L. and Ragsdale, C. W. (1998). The hem of the embryonic cerebral cortex is defined by the expression of multiple Wnt genes and is compromised in Gli3-deficient mice. *Development* **125**, 2315-25.

Huang, X., Ketova, T., Fleming, J. T., Wang, H., Dey, S. K., Litingtung, Y. and Chiang, C. (2009). Sonic hedgehog signaling regulates a novel epithelial progenitor domain of the hindbrain choroid plexus. *Development* **136**, 2535-43.

Iulianella, A., Sharma, M., Durnin, M., Vanden Heuvel, G. B. and Trainor, P. A. (2008). Cux2 (Cutl2) integrates neural progenitor development with cell-cycle progression during spinal cord neurogenesis. *Development* **135**, 729-41.

Johansson, P. A. (2014). The choroid plexuses and their impact on developmental neurogenesis. *Front Neurosci* **8**, 340.

Johansson, P. A., Irmler, M., Acampora, D., Beckers, J., Simeone, A. and Gotz, M. (2013). The transcription factor Otx2 regulates choroid plexus development and function. *Development* **140**, 1055-66.

Liddelow, S. A. (2015). Development of the choroid plexus and blood-CSF barrier. *Front Neurosci* **9**, 32.

Liddelow, S. A., Dziegielewska, K. M., Vandeberg, J. L. and Saunders, N. R. (2010). Development of the lateral ventricular choroid plexus in a marsupial, Monodelphis domestica. *Cerebrospinal Fluid Res* **7**, 16.

Lun, M. P., Monuki, E. S. and Lehtinen, M. K. (2015). Development and functions of the choroid plexus-cerebrospinal fluid system. *Nat Rev Neurosci* **16**, 445-57.

McNeil, E., Capaldo, C. T. and Macara, I. G. (2006). Zonula occludens-1 function in the assembly of tight junctions in Madin-Darby canine kidney epithelial cells. *Mol Biol Cell* **17**, 1922-32.

Monuki, E. S., Porter, F. D. and Walsh, C. A. (2001). Patterning of the dorsal telencephalon and cerebral cortex by a roof plate-Lhx2 pathway. *Neuron* **32**, 591-604.

Moore, S. A. and Iulianella, A. (2021). Development of the mammalian cortical hem and its derivatives: the choroid plexus, Cajal-Retzius cells and hippocampus. *Open Biol* **11**, 210042.

Ozcelik, M., Cotter, L., Jacob, C., Pereira, J. A., Relvas, J. B., Suter, U. and Tricaud, N. (2010). Pals1 is a major regulator of the epithelial-like polarization and the extension of the myelin sheath in peripheral nerves. *J Neurosci* **30**, 4120-31.

Roy, A., Gonzalez-Gomez, M., Pierani, A., Meyer, G. and Tole, S. (2014). Lhx2 regulates the development of the forebrain hem system. *Cereb Cortex* **24**, 1361-72.

Schindelin, J., Arganda-Carreras, I., Frise, E., Kaynig, V., Longair, M., Pietzsch, T., Preibisch, S., Rueden, C., Saalfeld, S., Schmid, B. et al. (2012). Fiji: an open-source platform for biological-image analysis. *Nat Methods* **9**, 676-82.

Stanton-Turcotte, D., Hsu, K., Moore, S. A., Yamada, M., Fawcett, J. P. and Iulianella, A. (2022). Mllt11 Regulates Migration and Neurite Outgrowth of Cortical Projection Neurons during Development. *J Neurosci* **42**, 3931-3948.

Yamada, M., Clark, J. and Iulianella, A. (2014). MLLT11/AF1q is differentially expressed in maturing neurons during development. *Gene Expr Patterns* **15**, 80-7.

Yamada, M., Clark, J., McClelland, C., Capaldo, E., Ray, A. and Iulianella, A. (2015). Cux2 activity defines a subpopulation of perinatal neurogenic progenitors in the hippocampus. *Hippocampus* **25**, 253-67.

FIGURE LEGENDS

Figure 1. *Mllt11* loss alters development of dorsal telencephalic midline structures.
(A, B) Coronal sections of DTM region at E14.5 WT control vs. *Cux2*$^{iresCre/+}$driven *Mllt11* cKO stained for Lhx2 (white) counterstained with DAPI (blue). (C) Scatter boxplot identifying the total number of Lhx2^{+} cells per 50 μm^{2}. *Mllt11* cKOs displayed a significant increase in Lhx2^{+} cells in the dorsal medial telencephalon relative to WTs (p=0.0004, n=6). (D, E) Coronal sections of medial telencephalon of E14.5 WT vs. cKO stained for Otx1/2 (white) to label the CH region and ChP. (F) Scatter boxplot identifying the total CH area in μm^{2}. A significant decrease is observed in the CH area in the cKO in comparison to WT controls (p= 0.003; n=6). (G, H) Coronal sections of forebrains from E14.5 WT vs. cKO embryos with tdTomato (red; Ai9 reporter) fluorescence as a readout for *Cux2*$^{iresCre/+}$-mediated recombination in the CH and ChP stalk. White arrowheads depict tdTomato^{+} fate-mapped NEPs contributing to ChP formation. Quantification of data presented as mean ± SEM. Abbreviations: CH, cortical hem; ChP, choroid plexus; DNE; dentate neuroepithelium; hf, hippocampal fissure, lv, lateral ventricle.

Figure 2. *Mllt11* loss results in truncated telencephalic ChP due to altered neuroepithelial migration.
(A, B) Cross sections of telencephalic ChPs from 3 different individual WT controls and *Mllt11* cKO fetuses at E14.5 stained for Otx1/2 to label the ChP. (C) Scatter boxplot of ChP stalk length in μm. ChP stalk length was significantly shorter in the cKOs (407.0 ± 22.95μm; n=9) relative to WTs (540.1 ± 27.04μm; n=8; P=0.0018). (D) Scatter boxplot quantifying ChP stalk thickness in μm. cKO fetuses (29.33 ± 1.57μm, n=8) displayed no significant difference in ChP thickness relative to WTs (26.17 ± 0.93μm; P= 0.10). (E) Bar chart quantifying total Otx1/2^{+} cells per 50 μm^{2}, beginning at the base of the ChP stalk and counted in 50μm increments. Quantification of data presented as mean ± SEM. Abbreviations: ChP, Choroid Plexus, SEM, standard error of the mean.

Figure 3. *Mllt11* loss alters the epithelial anatomy of the choroid plexus.
(A-D) Cross-sectional view of WT and *Mllt11* cKO telencephalic ChP stained for ZO-1 (yellow) and DAPI (blue). Solid green arrowheads (D) identify the disorganized placement of cKO ChP

epithelial cells relative to the single cell layer organization of WT ChP. (E) Scatter boxplot identifying Otx1/2^{+}/EdU^{+} cells per ChP stalk, reporting a significant decrease in cKOs (p= 0.015, n=3) following an EdU pulse at E14.5 and analysis at E18.5. (F) Scatter boxplot identifying the percent total of Otx1/2^{+}/EdU^{+} cells in the dorsal arm of the stalk and the ventral arm of the stalk, reporting a significant decrease in percent of Otx1/2^{+}/EdU^{+} in the ventral arm of the cKOs relative to the dorsal arm (p= 0.005, n=3) at E18.5. (G-H) Cross section of WT and cKO ChP strained for Otx1/2 (yellow) and EdU (violet) at E18.5 (EdU pulse at E14.5). Solid and open green arrowheads identify Otx1/2^{+}/EdU^{+} cells in the dorsal arm and the ventral arm of the stalk, respectively. Scale bar = 50µm. Quantification of data presented as mean ± SEM. Abbreviations: ChP, Choroid Plexus.

Figure 4. *Mllt11* cKOs displayed loss of cuboidal cytoarchitecture of the ChP stalk epithelium.

Coronal sections of the proximal and distal regions of the ChP in WT and *Mllt11* cKO mice stained for Pals1. (B-E) Bar graphs depicting no significant differences in mean fluorescence levels of or percentage of area containing Pals1 staining respectively, quantified proximally (B, C) or distally (D, E). (F, G) Scatter boxplots quantifying a significant increase in ChP thickness (F) proximally in *Mllt11* cKO (24.99µm ± 1.37; n=4) compared to WT (15.08µm ± 0.81; n=4; P=.002), with no significant differences seen (G) distally. White boxes indicate sites of insets. Red boxes indicate example regions sampled for analysis of immunofluorescence. Red lines indicate sample regions measured for thickness analysis. Scale bar = 50µm. Quantification of data presented as mean ± SEM. Abbreviations: ChP, choroid plexus.

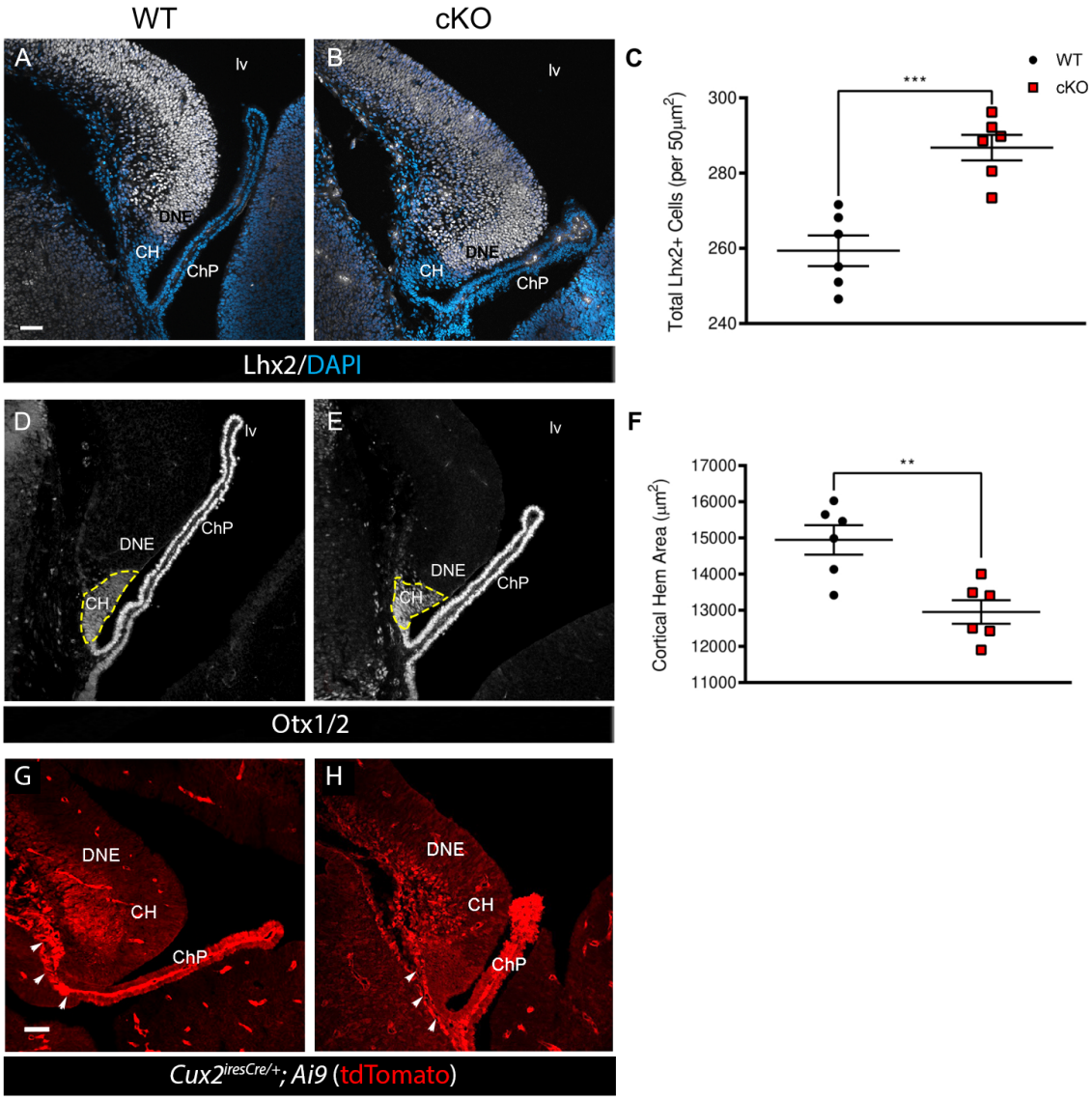
WT
cKO
A
B
lv
DNE
CH
ChP
Lhx2/DAPI
C
WT
cKO
***
Total Lhx2+ Cells (per 50μm²)
300
280
260
240
D
E
Otx1/2
F
**
Cortical Hem Area (μm²)
17000
16000
15000
14000
13000
12000
11000
G
H
Cux2iresCre/+; Ai9 (tdTomato)

Figure 1

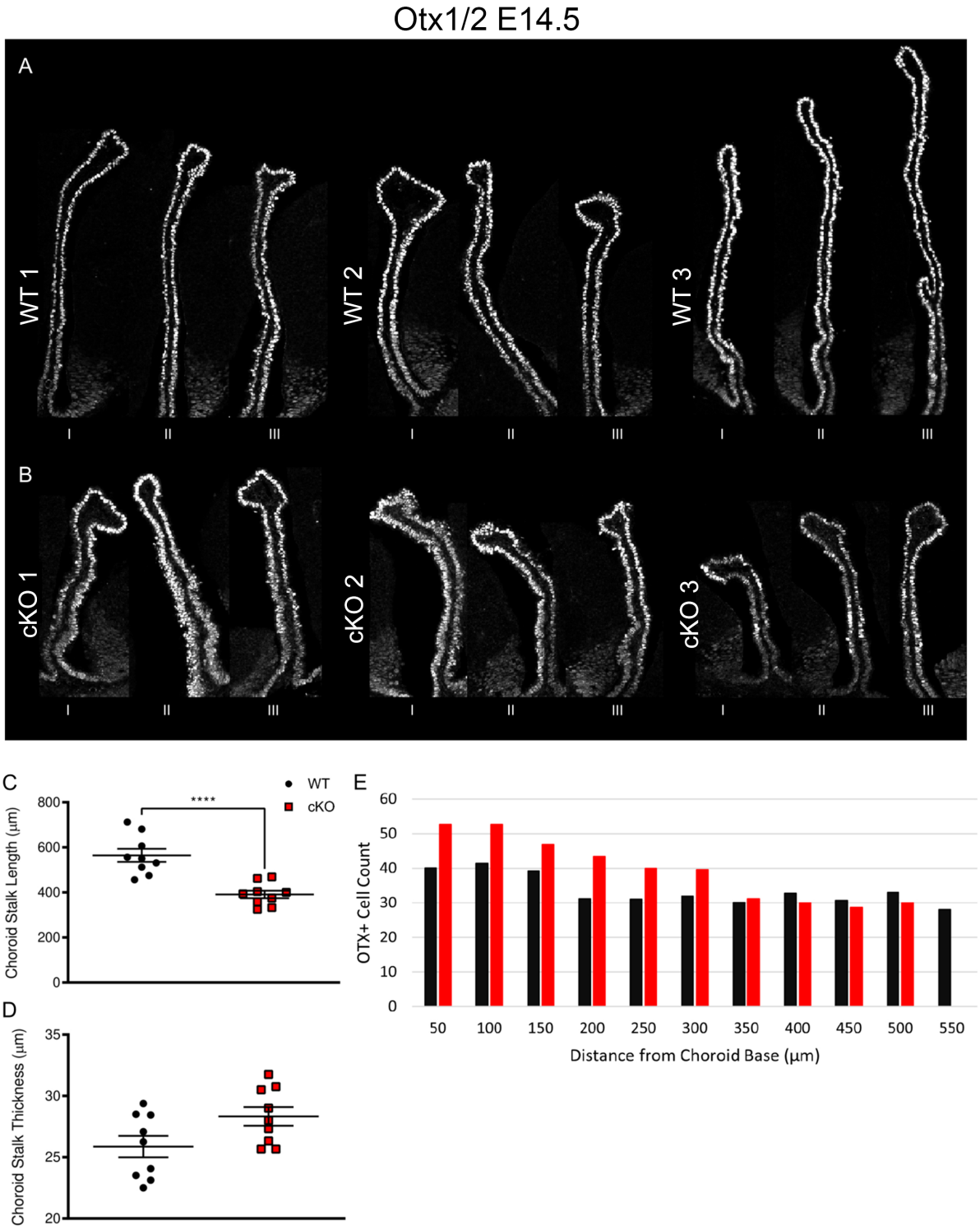
Otx1/2 E14.5
A
WT 1
WT 2
WT 3
I
II
III
B
cKO 1
cKO 2
cKO 3
C
WT
cKO
****
Choroid Stalk Length (µm)
800
600
400
200
0
D
Choroid Stalk Thickness (µm)
35
30
25
20
E
OTX+ Cell Count
60
50
40
30
20
10
0
50
100
150
200
250
300
350
400
450
500
550
Distance from Choroid Base (µm)

Figure 2

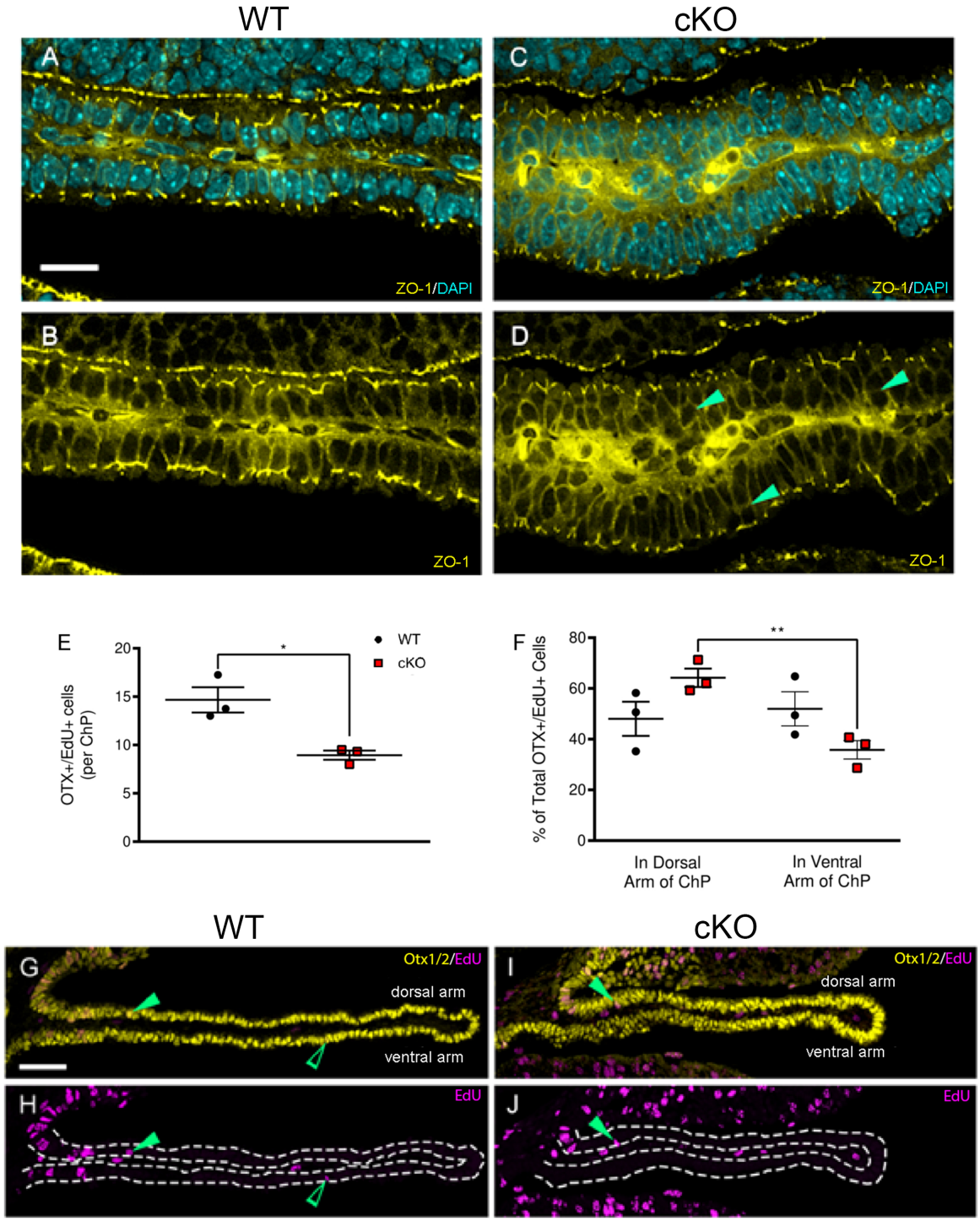
WT
cKO
A
C
ZO-1/DAPI
ZO-1/DAPI
B
D
ZO-1
ZO-1
E
OTX+/EdU+ cells (per ChP)
20
15
10
5
0
*
WT
cKO
F
% of Total OTX+/EdU+ Cells
80
60
40
20
0
**
In Dorsal Arm of ChP
In Ventral Arm of ChP
WT
cKO
G
Otx1/2/EdU
dorsal arm
ventral arm
I
Otx1/2/EdU
dorsal arm
ventral arm
H
EdU
J
EdU

Figure 3

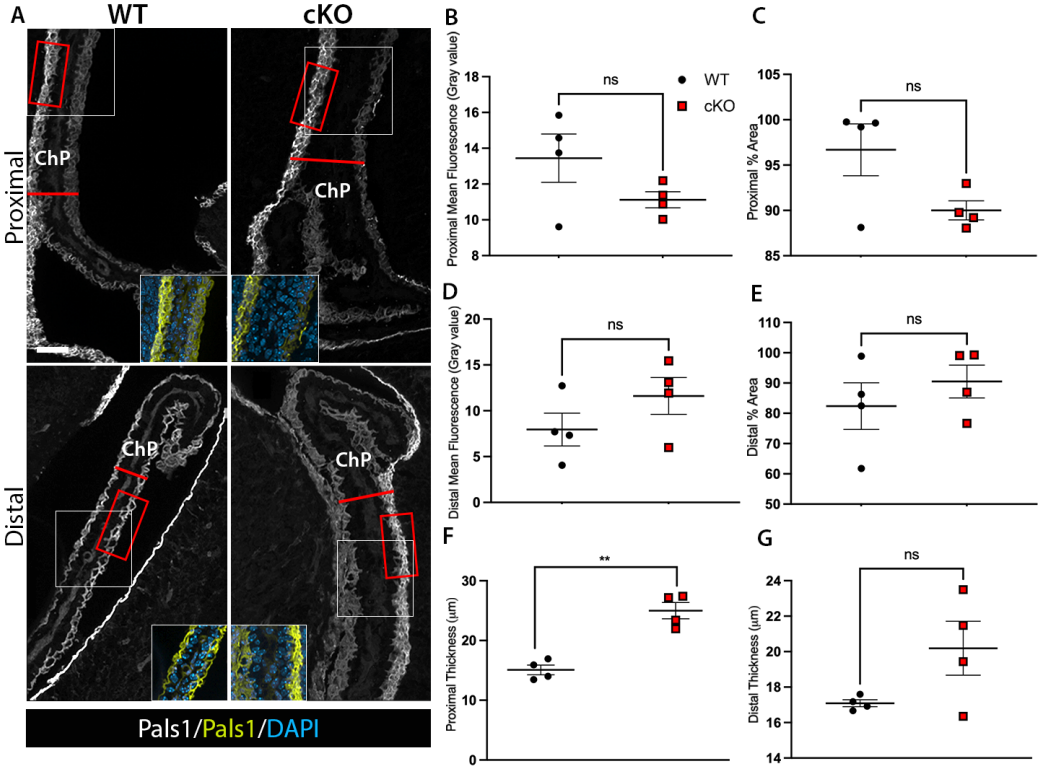
A
WT
cKO
Proximal
Distal
ChP
Pals1/Pals1/DAPI
B
Proximal Mean Fluorescence (Gray value)
ns
WT
cKO
C
Proximal % Area
D
Distal Mean Fluorescence (Gray value)
E
Distal % Area
F
Proximal Thickness (µm)
**
G
Distal Thickness (µm)

Figure 4